M^{3+} Lanthanide Cation Solvation by Acetonitrile: The Role of Cation Size, Counterions, and Polarization Effects Investigated by Molecular Dynamics and Quantum Mechanical Simulations

M. Baaden,[†] F. Berny,[†] C. Madic,[‡] and G. Wipff*,[†]

Institut de Chimie, Université Louis Pasteur, UMR CNRS 7551, 4, rue B. Pascal, 67 000 Strasbourg, France and Commissariat à l'Energie Atomique, BP 171, 30207 Bagnols-sur-Cèze Cédex, France

Received: April 7, 2000

We report a molecular dynamics (MD) study on M^{3+} lanthanide (La^{3+}, Eu^{3+}, and Yb^{3+}) cations in dry acetonitrile solution and in $M(MeCN)_n^{3+}$ clusters ($n = 1-15$) where two classical force-field representations of the cations are compared, in conjunction with the OPLS model of acetonitrile. It is shown that a set of van der Waals cation parameters (*set2*) fitted from free energies of hydration overestimates the cation coordination numbers (*CN*s). Another set of parameters (*set1*), where the size of cations is scaled down by $2^{1/6}$ (using the σ van der Waals value for R^*) yields better results. Quantum mechanical calculations performed on $M(MeCN)_n^{3+}$ aggregates ($n = 1-9$) demonstrate the importance of charge-transfer and polarization effects. They confirm the preferred coordination number of eight for Yb^{3+}, the $Yb(MeCN)_{8+1}^{3+}$ species with one MeCN molecule in the outer coordination sphere being somewhat more stable than $Yb(MeCN)_9^{3+}$ D_{3h}. Adding a polarization term for the 1−6−12 OPLS acetonitrile to the force field (*set2*+*pol*) indeed markedly improves the calculated *CN*s. In all MD simulations, a remarkable dynamic feature is observed in the first solvation shell where the lifetime of acetonitrile molecules increases from Yb^{3+} to La^{3+}, that is, inversely to the cation−solvent interaction energies and to the aqueous phase behavior. Rare-earth salts with ClO_4^- and $F_3CSO_3^-$ anions and the question of ion binding selectivity by **L** ligands (formation of ML_3^{3+} complexes, where **L** is a pyridine−dicarboxamide ligand) in acetonitrile solution are investigated by free-energy perturbation simulations, comparing the *set1*, *set2*, and *set2*+*pol* models. It is found that selectivities are markedly determined by the change in solvation-free energies of the uncomplexed cations, with pronounced counterion effects. The two simplest models (*set1* or *set2* without polarization) predict the correct order of complexation ($Yb^{3+} > Eu^{3+} > La^{3+}$), whereas addition of polarization contribution leads to the inverse order, because of overestimation of the cation−anion interactions in the salt solutions.

I. Introduction

Characterization of solvation properties of lanthanide cations represents an important theme per se, but also is a reference for further studies on cation complexation, because first shell solvent molecules generally are replaced by binding sites of the ligand upon complexation.[1] It is therefore crucial to identify the solvation patterns of uncomplexed cations. So far, most of the experimental studies focused on water as solvent.[2] Nonaqueous polar solvents, such as dimethylsulfoxide (DMSO), amides, alcohols, nitromethane, or acetonitrile, where lanthanide salts are soluble, received less attention.[3,4] As shown for alkaline and alkaline earth cations,[5−7] computer simulations contribute to our understanding of ion solvation. Aqueous solutions of M^{3+} lanthanide cations have been simulated by Monte Carlo methods[8,9] or molecular dynamics (MD).[10−12] Recently, following a procedure developed for alkali and alkaline-earth cations,[13] van Veggel et al. fitted van der Waals parameters on the free energies of hydration of M^{3+} lanthanide cations,[9] using pairwise additive 1−6−12 potentials that can be used in common software such as AMBER, CHARMM, or BOSS. This set of parameters, referred to later as *set2*, also gives reasonable results for the $M^{3+\cdots}O_{water}$ distances and for the corresponding hydration numbers. With the exception of the methanol solution,[9] the performance of these parameters in a nonaqueous solvent environment has not been established. We therefore decided to compare the solvation patterns of lanthanide cations of decreasing size (La^{3+}, Eu^{3+}, Yb^{3+}) in acetonitrile solution, using the widely used OPLS model fitted on the properties of the pure liquid phase for the solvent.[14] For the cation, two sets of Lennard−Jones parameters are compared, with "small" (*set1*) and somewhat larger cation radii (*set2*), respectively. In addition, given the importance of polarization effects induced by the hard and highly charged cations,[12,15] we investigate the role of solvent polarization, using the *set2* of cation parameters in conjunction with the OPLS model of acetonitrile, to which polarization energy contributions have been added (*set2*+*pol* model).

There are few experimental results that can be used to assess the quality of the simulated lanthanide models. In contrast to aqueous solvation, the cation solvation numbers (*CN*s) and the corresponding $M^{3+\cdots}N_{MeCN}$ distances have not been determined consistently in acetonitrile solution. Solid-state structures, however, may provide valuable information of the cation solvation.[23,24] Concerning hydration, $M^{3+\cdots}O_{H_2O}$ distances determined in aqueous solution [by X-ray, extended X-ray absorption fine structure (EXAFS), or neutron diffraction techniques[16−20]] are within 0.1 Å the same as in the solid-state structures,[21,22] and the *CN*s differ by at most one unit for a given

[†] Université Louis Pasteur.
[‡] Commissariat à l'Energie Atomique.

10.1021/jp001352v CCC: $19.00
Published on Web 07/25/2000

ion. Recently, Deacon et al.[25] described the solid-state structure of $Yb(MeCN)_8^{3+}$ and $M(MeCN)_9^{3+}$ (M = Pr; Sm; La) homoleptic lanthanoid complexes.[25] In this series, the cation coordination numbers range from 8 to 9 (as do the corresponding hydration numbers), whereas the average $M^{3+}\cdots N_{MeCN}$ distances increase from 2.39 to 2.63 Å. Athough the coordination polyhedron in solution may differ somewhat from the one in the solid state,[26] one can reasonably assume that these structures depict the behavior of the "naked" cations in acetonitrile solution. Because the characteristics of the first solvation shell may be influenced by long-range forces, we also simulated $M(MeCN)_{15}^{3+}$ clusters with M = La, Eu, Yb, whose first shell is saturated, allowing for exchange with MeCN molecules of the second shell. Further insights into ion−acetonitrile interactions will be presented from quantum mechanical calculations on $M(MeCN)_n^{3+}$ aggregates.

An important difference of acetonitrile, compared with aqueous solution is the status of neutralizing counterions, some of them remaining in close contact with the M^{3+} cation.[3] We thus next examine the role of perchlorate and triflate counterions, where the $M(ClO_4)_3$ and $M(F_3CSO_3)_3$ salts are simulated in acetonitrile. We want to investigate whether simulations starting from intimate or dissociated ion pairs converge to similar ion-pairing patterns. The structural features of simulated intimate ion pairs will be described shortly.

Another important aspect of solvation concerns the energetics, which is cation and model dependent. To our knowledge, no related experimental data for M^{3+} ions in nonaqueous solvents are available. Thus, computational results have to be compared from one model to another one. Using free-energy perturbation (FEP) calculations, we calculate the solvation free-energy differences between La^{3+}, Eu^{3+}, and Yb^{3+} as a function of the cation model (*set1* vs *set2* vs *set2*+*pol*). This is first achieved in the absence of counterions in bulk acetonitrile solution, as well as in the $M(MeCN)_{15}^{3+}$ clusters for comparison. Then, FEP simulations are reported in solution in the presence of neutralizing counterions. Finally, the question of ion-binding selectivity in a recently characterized $M\mathbf{L}_3^{3+}$ complex (**L** is a pyridine dicarboxamide ligand) will be presented.

II. Methods

Molecular Dynamics. The MD simulations were performed with the AMBER4.1 software[27] where the potential energy U is given by:

$$U = \Sigma_{\text{bonds}} K_r(r - r_{eq})^2 + \Sigma_{\text{angles}} K_\theta(\theta - \theta_{eq})^2 + \Sigma_{\text{dihedrals}}\Sigma_n V_n(1 + \cos n\phi) + \Sigma_{i<j}\left[q_i q_j/R_{ij} - 2\epsilon_{ij}(R_{ij}^*/R_{ij})^6 + \epsilon_{ij}(R_{ij}^*/R_{ij})^{12}\right] \quad (1)$$

The electrostatic and van der Waals interactions between nonbonded atoms are described within a pairwise additive scheme by a 1−6−12 potential. Parameters for the solutes were taken from the AMBER force field[28] and from previous studies. Two sets of Lennard−Jones parameters (*set1* and *set2*) were used for the La^{3+}, Eu^{3+}, and Yb^{3+} cations. The *set2* has been developed ($R^*_{La} = 2.105$; $R^*_{Eu} = 1.852$; $R^*_{Yb} = 1.656$ Å; $\epsilon_{La} = 0.06$; $\epsilon_{Eu} = 0.05$; $\epsilon_{Yb} = 0.04$ kcal/mol)[9] to reproduce the free energies of hydration of these cations. We derived *set1* from *set2* by scaling down the R^* radii by $2^{1/6}$, using thus the original σ values for R^* ($R^*_{La} = 1.875$; $R^*_{Eu} = 1.650$; $R^*_{Yb} = 1.475$ Å) and keeping the same ϵ parameters as in *set2*. Thus, the cation size increases from *set1* to *set2*. The acetonitrile solvent was modeled with the OPLS model fitted by Jorgensen and Briggs[14] on the bulk liquid properties. The Lorentz−Berthelot mixing rules were used for unlike atoms: $\epsilon_{ij} = (\epsilon_{ii} * \epsilon_{jj})^{1/2}$ and $R^*_{ij} = R^*_i + R^*_j$.

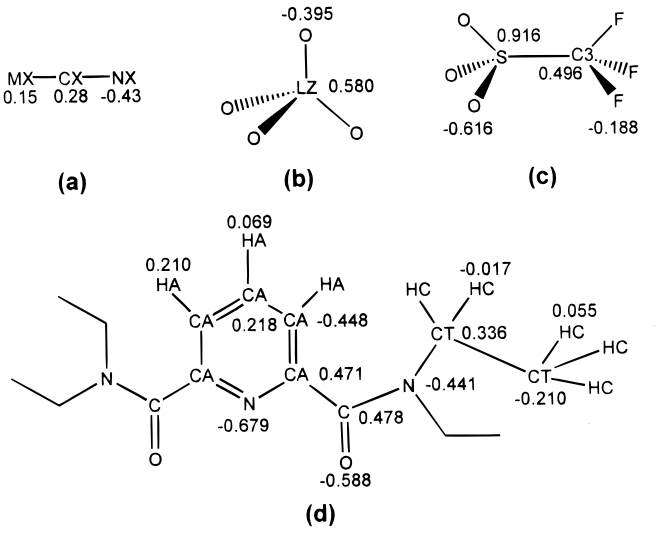

Figure 1. Atomic charges and AMBER atom types on MeCN (a), ClO_4^- (b), $F_3CSO_3^-$ (c) and the pyridine−dicarboxamide ligand (d) used for the MD simulations.

The atomic charges used for the ClO_4^- and $F_3CSO_3^-$ anions have been fitted on electrostatic potentials calculated at the HF level on the optimized structures with a 6-31G* basis set. They are given in Figure 1 with the corresponding AMBER atom types. In a third energy representation of the system (referred to as *set2* + *pol*) we used the *set2* parameters for M^{3+} cations while adding polarization terms to the OPLS acetonitrile model and to the anions. The polarization energy was calculated as described in ref 29. The atomic polarizabilities used for the solvent ($\alpha_{Me} = 0.878$, $\alpha_N = 0.520$, and $\alpha_C(CN) = 0.360$ Å^3) and on the anions ($\alpha_O = 0.434$, $\alpha_S = 1.70$, $\alpha_{Cl} = 1.91$, $\alpha_F = 0.32$, $\alpha_C = 0.616$ Å^3) were adapted from Applequist et al.[30] A residue-based 12/15 Å twin cutoff was applied to the nonbonded interactions, using 3D periodic boundary conditions. Some tests with PME Ewald correction of the long-range electrostatics have been performed on the $M(ClO_4)_3$ salts.

The characteristics of the simulated systems are described in Table S1. A typical solvent box is shown in Figure 2. After 1000 steps of energy minimization, MD simulations were performed at constant volume and at a temperature maintained at 300 K by coupling to a thermal bath with a relaxation time of 0.1 ps. The solvent bonds were constrained with SHAKE, using a time step of 1 fs.

FEP calculations were performed to calculate the difference in Helmholtz free energies (ΔG) between two systems, using the windowing technique, based on the following equations:

$$\Delta G = \Sigma \Delta G_\lambda \quad \text{and} \quad \Delta G_\lambda = RT \log\left\langle \exp\frac{(U_\lambda - U_{\lambda+\Delta\lambda})}{RT}\right\rangle_\lambda$$

The mutations from one cation to the other (or from one model to the other) were achieved in 51 equally spaced windows, performing at each window (i.e., at each λ) 2 ps of equilibration and 3 ps of data collection. The variations of the potential energy U_λ were calculated using a linear combination of the ϵ_{ij} and R_{ij}* parameters of the initial state ($\lambda = 1$) and the final state ($\lambda = 0$):

$$\epsilon(\lambda) = \lambda\epsilon(1) + (1 - \lambda)\epsilon(0) \quad \text{and} \quad R^*(\lambda) = \lambda R^*(1) + (1 - \lambda)R^*(0)$$

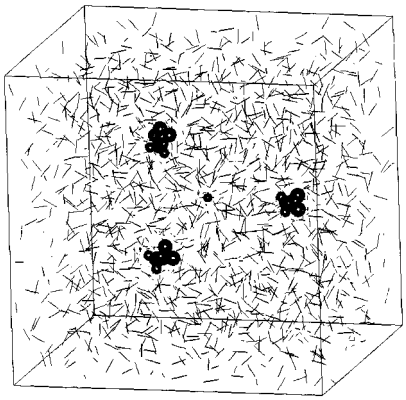

Figure 2. Acetonitrile box with the dissociated Eu^{3+} triflate salt. Characteristics of the simulated systems are given in Table S1.

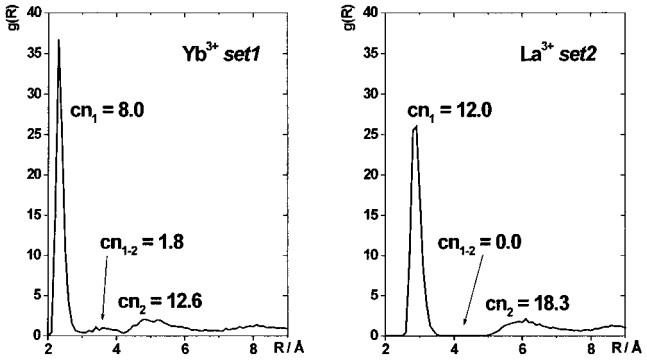

Figure 3. Radial distribution functions (RDFs) of N_{CN} around the Yb^{3+}-(*set1*) and La^{3+}(*set2*) cations and corresponding coordination numbers: cn_1 (first shell), cn_2 (second shell), and cn_{1-2} (intermediate shell, due to molecules exchanging between the first and second shell).

ΔG values were accumulated and averaged from "forward" (increasing λ) and "backward" (decreasing λ) calculated energies.

Analysis of MD Results. Average structural features and energy components were analyzed from the trajectories saved every 0.2−0.5 ps using the MDS and DRAW software.[31,32]

Quantum Mechanics (QM). The QM ab initio calculations on $M(MeCN)_n^{3+}$ aggregates were performed at the HF level using the Gaussian-94[33] and Gaussian-98 packages.[34] The 46 + $4f^n$ core electrons of the lanthanide cations were described by the quasi-relativistic effective core potential (ECP) of Dolg et al.[35,36] and the valence electrons by a (7s,6p,5d)/[5s,4p,3d] Gaussian basis set supplemented by one f polarization function of exponent 0.591.[37] The H, C, and N atoms of MeCN were described by the standard Dunning−Hay double-ζ basis set.[38] The $M(MeCN)_n^{3+}$ systems were fully optimized, without imposing symmetry. The $M(MeCN)_3^{3+}$ species moved from D_{3h} to C_{3v}, as noticed in related systems.[39] For $n = 8$ and 9 we started with the X-ray structure of the $La(MeCN)_9^{3+}$ and $Yb(MeCN)_8^{3+}$ complexes.[25] For the $Yb(MeCN)_9^{3+}$ and $Yb(MeCN)_{8+1}^{3+}$ complexes, optimizations were repeated with the density functional theory (DFT) method using the B3LYP functional.

III. Results

We mainly focus on the comparison of the simulation results obtained with the *set1*, *set2*, and *set2*+*pol* parameters. We first consider structural features for uncomplexed M^{3+} cations in the absence of neutralizing counterions as a reference state. Then the cation solvation of lanthanide salts is compared with two types of neutralizing counterions (perchlorate ClO_4^- and triflate $F_3CSO_3^-$, respectively) from a structural point of view. We next move to energy features and compare the change in solvation free energies in the cation series as a function of the model used for the cation (*set1* vs *set2*) and for the solvent (OPLS vs polarized OPLS model, used with the *set2* cation parameters, noted hereafter *set2*+*pol*).

1. Characteristics of M^{3+} Cation Solvation in Acetonitrile (No Counterion): Static and Dynamic Aspects. Cation Coordination Numbers. Because the size and behavior of Eu^{3+} are intermediate between those of Yb^{3+} and La^{3+}, we mainly consider the latter. The $M^{3+}\cdots N_{MeCN}$ solvent radial distribution functions (RDFs) of Yb^{3+}(*set1*) and La^{3+}(*set2*) in solution are shown in Figure 3. They show a first narrow peak, followed by more diffuse peaks. In the largest modeled cation, La^{3+}(*set2*), the RDF drops to zero between the first peak (at 2.85 Å) and the broad second one (at about 6 Å), which indicates the absence of solvent exchange between the first and second shell during the whole simulation (1 ns). This feature contrasts with the smallest simulated cation, Yb^{3+}(*set1*), whose RDF displays a smooth hump between the first shell peak (at 2.30 Å) and the second shell (at about 5.10 Å), indicating solvent exchange between the two shells. This exchange is visualized in Figure 4, which shows a cumulated view of solvent molecules during the last 0.2 ns. It confirms the lack of exchange around La^{3+}(*set2*) and the extensive exchange around Yb^{3+}(*set1*), some of the MeCN molecules diffusing from far beyond the second shell.

The running coordination numbers of the La^{3+}, Eu^{3+}, and Yb^{3+} cations, obtained by stepwise integration of the RDFs, are plotted in Figure 5. For the La^{3+}(*set2*) cation, the horizontal plateau between 3.3 and 4.8 Å confirms the lack of solvent exchange with *set2*, whereas with all other models, as well as with all other cations, the positive slope indicates some solvent exchange between the first and second shell. This feature is quite surprising, if one refers to the water coordination case, where according to experimental and simulation data,[12,40] the lifetime of solvent coordination decreases from Yb^{3+} to La^{3+}, following the decrease of ion−water interactions. According to the energy component analysis (Table S2), the $M^{3+}\cdots$acetonitrile interaction energies also decrease from Yb^{3+} to La^{3+} with both sets of cation parameters, whereas solvent−solvent attractions remain comparable.

In Table 1 are reported the cn_1 and cn_{1-2} coordination numbers of MeCN molecules, which correspond, respectively, to the first sharp peak of the RDFs (inner coordination sphere) and to the smooth hump of the exchanging solvent molecules (see Figure 3), as well as the average total number $\langle CN \rangle$ of "first shell" solvent molecules, where $\langle CN \rangle = cn_1 + cn_{1-2}$. For a given cation, the coordination number is markedly model-dependent. For Yb^{3+}(*set1*), the total $\langle CN \rangle$ is 9.8, including the contribution of the 1.8 molecules in the "intermediate shell" and a cn_1 number of 8.0 as in the solid state.[25] With the *set2* parameters, the $\langle CN \rangle$ of Yb^{3+} would be too high (8.5 + 1.0), as would be the $\langle CN \rangle$ of La^{3+} (12 + 0). Thus, the *set2* parameters lead to an overestimation of the CNs in acetonitrile, when used with the standard OPLS model. When polarization energy is added to acetonitrile (compare *set2* and *set2*+*pol* models), the total coordination numbers $\langle CN \rangle$ of Yb^{3+} and La^{3+} decrease to 8.75 and 9.80, respectively, mostly because of the decrease of solvent molecules in the first shell ($\Delta cn_1 = 0.50$ and 2.25, respectively). The resulting cn_1 values of 7.95 and 9.75 become closer to the experimental *CN*s of 8 and 9, respectively. As the size of the cation increases, the three models lead to the same qualitative

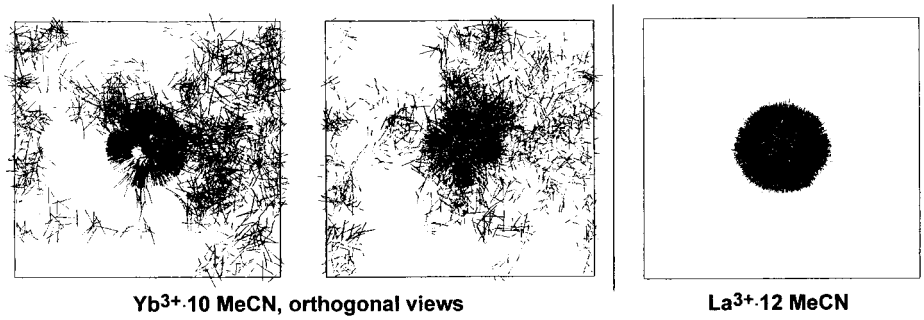

Figure 4. Cumulated views of MeCN molecules around the Yb^{3+}(*set1*) and La^{3+}(*set2*) cations during the last 0.2 ns, based on a selection of solvent molecules which sit in the first solvation shell at the end of the dynamics (1 ns).

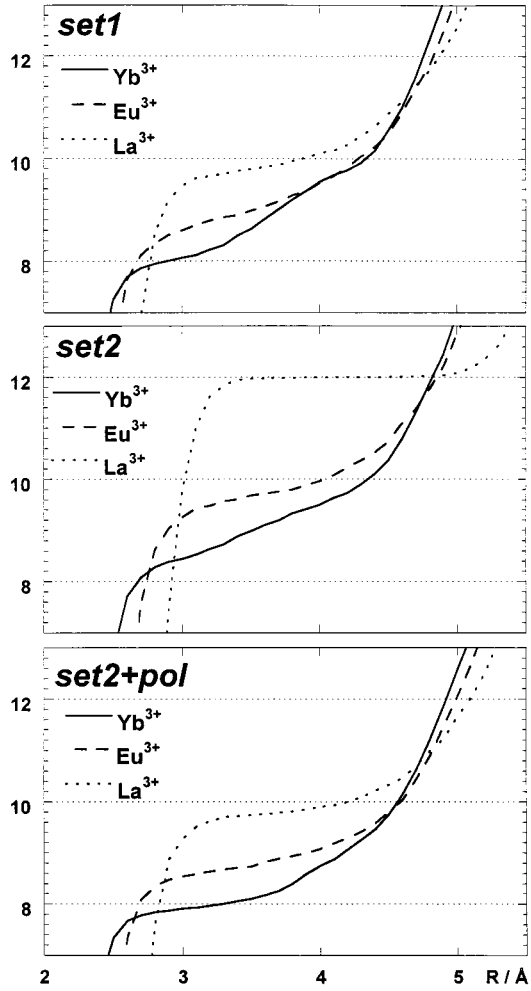

Figure 5. Yb^{3+}, Eu^{3+}, La^{3+} cations in acetonitrile solution. Running coordination numbers as a function of the distance R (Å) from the cation. From MD simulations with *set1* (top), *set2* (middle), and *set2*+*pol* (bottom).

conclusion concerning the acetonitrile exchange, that is, a decrease from Yb^{3+} to La^{3+} (see cn_{1-2} in Table 1 and Figure 5).

Concerning the cn_1 number of inner sphere solvent molecules, we notice that some values are close to an integer number [e.g., 8 for Yb^{3+} with *set1* and *set2*+*pol* models, or 12 for La^{3+}(*set2*)]. In other cases, cn_1 is a noninteger. For instance, Eu^{3+}(*set1*) and Yb^{3+}(*set2*) have cn_1 close to 8.5, whereas La^{3+}(*set1*) or La^{3+}(*set2*+*pol*) have cn_1 close to 9.7. Following the procedure of Kowall et al.,[12] we therefore dissected the contributions of the acetonitrile molecules in the inner shell (cn_1), second sphere (cn_2), and intermediate shell (cn_{1-2}), as a function of their *instantaneous* distances with M^{3+}. The resulting distribution (Figure 6) confirms that integer numbers of cn_1 correspond to a unique type of coordination, whereas noninteger cn_1 numbers correspond to contribution of two types of coordination only. This contrasts with the second shell, whose average composition cn_2 results from a large number of coordination types (e.g., for La^{3+}(*set1*) the 14.9 value of cn_2 results from an average of 12−18 coordinated species). In the intermediate shell, several contributions may be similarly recognized. For instance, for Yb^{3+}(*set2*) the cn_{1-2} average number of 1.05 results from nearly equally populated forms having 0, 1, and 2 solvent molecules, respectively, instead of a dominant population of 1.

Cation−Acetonitrile Distances. With the three models, the average M^{3+}···solvent distances in the first coordination shell, determined by R_{max} (the maximum of the first peak in the RDFs), increase from Yb^{3+} to La^{3+}, following the cation radii (by about 0.30 Å with *set1*, 0.45 Å with *set2*, and 0.4 Å with *set2*+*pol*). For a given cation, R_{max} is also larger with *set2* than with *set1* (by about 0.10 Å for Yb^{3+} and 0.25 for La^{3+}). In keeping with the fact that Yb^{3+}(*set2*) and Eu^{3+}(*set1*) cation models have close R^* van der Waals radii, the corresponding R_{max} values are very close (2.40 and 2.45 Å, respectively). When acetonitrile polarization is added to the model (*set2*+*pol* parameters), R_{max} somewhat shortens (by about 0.1 Å), as expected from enhanced interactions with the cation (Table S2). Another characteristic distance is the average distance $\langle d_1 \rangle$ of the cn_1 molecules which sit *instantaneously* in the first shell. $\langle d_1 \rangle$ values are about 0.08 Å larger than the corresponding R_{max} ones and follow the same trends. Again, this small difference is in the order of statistical fluctuations.

We now compare the calculated MeCN···M^{3+} distances with the average values determined in the solid state for Yb-$(MeCN)_8^{3+}$ (2.39 Å) and La$(MeCN)_9^{3+}$ (2.63 Å), as well as with data for other complexes retrieved from the Crystallographic Cambridge Structural Database.[41] The results displayed in Figure 7 show that in the latter complexes, the MeCN···M^{3+} distances are longer than those reported by Deacon et al.[25] This is due to the presence of neutralizing X^- counterions and ligands in the former case, where MeCN formally binds to a neutral MX_3 salt, and is therefore less attracted than by a "naked" M^{3+} cation. Steric effects caused by the coordinated ligands also weaken the cation−acetonitrile "bonds". Thus, Deacon's structures (details are given in Table S3) are most directly comparable with the simulated ones. Figure 7 makes clear that the *set2* parameters give the poorest agreement with experiment, whereas the *set1* gives the best. Thus, the parameters fitted on the hydration energies markedly overestimate the MeCN···M^{3+} distances, as well as the corresponding coordination numbers. Adding the acetonitrile polarization energy (*set2*+*pol* model) leads to a nice agreement for Yb^{3+}, but still yields

TABLE 1: M^{3+} Cations in Acetonitrile (No Counterions) and $M(MeCN)_{15}^{3+}$ Aggregates[a]

		RDF in acetonitrile			RDF for $M(MeCN)_{15}^{3+}$ aggregates		
solute	R^* [b]	R_{max}	$cn_1 + cn_{1-2}$[c]	$\langle CN \rangle$	R_{max}	$cn_1 + cn_{1-2}$[c]	$\langle CN \rangle$
Yb^{3+} *set1*	1.475	2.30	8.00 + 1.80	9.80			
Eu^{3+} *set1*	1.650	2.45	8.50 + 1.00	9.50			
La^{3+} *set1*	1.875	2.60	9.65 + 0.50	10.15			
Yb^{3+} *set2*	1.656	2.40	8.45 + 1.05	9.50	2.40	8.25 + 1.45	9.70
Eu^{3+} *set2*	1.852	2.60	9.60 + 0.35	9.95	2.60	9.30 + 0.40	9.70
La^{3+} *set2*	2.105	2.85	12.00 + 0.00	12.00	2.90	12.00 + 0.00	12.00
Yb^{3+} *set2+pol*	1.656	2.30	7.95 + 0.80	8.75	2.30	7.95 + 0.70	8.65
Eu^{3+} *set2+pol*	1.852	2.50	8.70 + 0.40	9.10	2.50	8.70 + 0.50	9.20
La^{3+} *set2+pol*	2.105	2.70	9.75 + 0.05	9.80	2.70	9.80 + 0.05	9.85

[a] Main characteristics of their first solvation shell, from the analysis of the RDFs. See Figure 3 for definitions of cn_1 (inner first shell) and cn_{1-2} (intermediate shell). [b] Cation van der Waals parameter in Å. [c] Number of MeCN in the first shell and in the intermediate shell

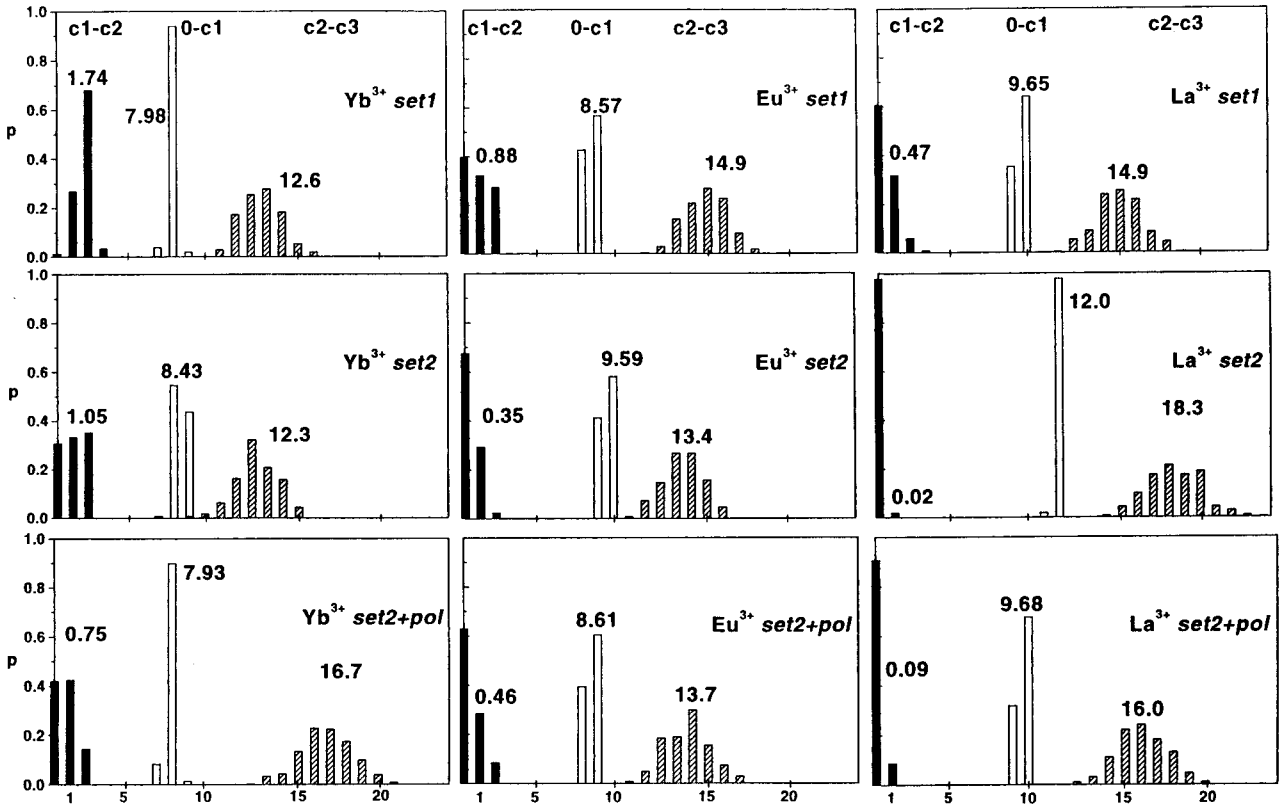

Figure 6. M^{3+} cations in acetonitrile (no counterions). Analysis of the first (0-c1) second (c2-c3), and intermediate (c1-c2) solvent shells, as defined by instantaneous distances taken from the RDFs. Populations of solvates as a function of the number of MeCN molecules instantaneously present in these shells.

distances that are too large for La^{3+}, which suggests that this modeled cation is somewhat too big.

It is instructive to compare the first shell characteristics in bulk solution with those in the $M(MeCN)_{15}^{3+}$ aggregates (Table 1). For a given cation and model, the RDFs of the solution and of the aggregate peak at the same R_{max} values, and the corresponding coordination number $\langle CN \rangle$ is nearly identical. The largest differences (about 0.3) are close to the statistical fluctuations. The average static characteristics of the first solvation shell in solution are thus not critically influenced by the second shell or more remote MeCN molecules. In the series of $Eu(MeCN)_n^{3+}$ aggregates ($n = 1-15$; Table 2), the average $MeCN\cdots Eu^{3+}$ distances increase by about 0.18 Å (*set2*) and 0.22 Å (*set2+pol*) when the number of solvent molecules increases from 1 to 15, because of the solvent−solvent repulsions in the first shell.

Orientation of Acetonitrile Molecules Induced by M^{3+} in Solution. In this section, we analyze the orientation of the acetonitrile molecules in the vicinity of the cation, as defined by the α-angle (< M−N−C; see Figure 8). At a given $M^{3+}\cdots N$ distance R, optimal charge−dipole interactions correspond to $\alpha = 180°$. Figure 8 represents the populations of MeCN molecules as a function of (α, R) parameters, where the N atoms were selected between spheres of radii R and $R + 0.25$ Å, centered on M^{3+}. Figure 8 reveals two well-defined zones for three cations and parameter sets, corresponding to the first and second shell, respectively. The α-orientation of first shell molecules (R between 3 and 4 Å) peaks as expected at 180°, but displays significant flexibility, of about ±40° in all cases. The second shell molecules (at about 6 Å) also display a marked orientation, which peaks near 150°. Then, a third shell is observed at about 9 Å for the three cations, where α peaks near 120° and displays still larger orientational flexibility (from about 40° to 170°).

Figure 8 gives another illustration of solvent exchange between the first and second shell. La^{3+}(*set2*) is the only case where no such exchange is observed during the simulation, and the two first "spots" corresponding to the first and second shell,

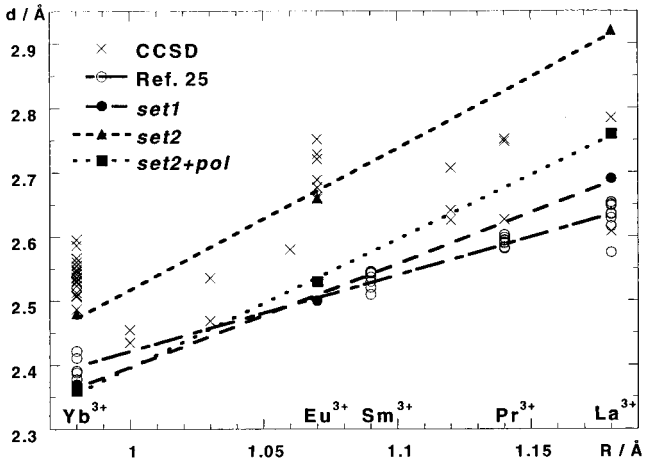

Figure 7. $MeCN\cdots M^{3+}$ distances (*d*, Å) as a function of the ionic radius (*R*, Å) for structures calculated in bulk acetonitrile solution (with *set1*, *set2*, and *set2*+*pol*), for those observed in the solid-state structures of Deacon et al.,[25] or those found in the Cambridge Crystallographic Structural Database (CCSD).[41]

respectively, are well separated. This is not the case for the other systems, in particular for Yb^{3+}(*set1*), where an important population of MeCN molecules between these two shells is seen clearly. The corresponding α-values are intermediate between those of the first and second shells, as anticipated.

Quantum Mechanical Optimization of $M(MeCN)_n^{3+}$ Aggregates. Comparison with MD Results. Force-field calculations do not take into account electronic and structural rearrangements of the ligands upon coordination. These effects are demonstrated by the QM optimizations of $Eu(MeCN)_n^{3+}$ (n = 1−9; Table 2), $La(MeCN)_n^{3+}$ and $Yb(MeCN)_n^{3+}$ aggregates (n = 1, 8, and 9; Table 3). According to these calculations, as n increases from 1 to 9, the $MeCN\cdots M^{3+}$ distance increases (by about 0.41 Å), whereas the geometric and electronic perturbations of the MeCN molecule with respect to the free ligand decrease.

Electronic perturbations are illustrated by changes in Mulliken charges. In all systems, the net charge on the cation is less than +3.0 e because of electron transfer Δq from all MeCN ligands. The transfer, mostly arising from the coordinated nitrogen atom, increases with the number n of ligands. For instance, in the $Eu(MeCN)_n^{3+}$ series, Δq increases from 0.23 (n = 1) to 1.10 e (n = 9), whereas the q_N charge changes from −0.64 to −0.10 e. For a given size of aggregate, Δq increases with the cation hardness. For instance, for n = 9, Δq is 0.71 for La and 1.34 e for Yb.

In most complexes (the only exception being $Eu(MeCN)_9^{3+}$ and $Yb(MeCN)_9^{3+}$) the q_N charge on the nitrogen atom is more negative than in the isolated MeCN molecule (q_N = −0.10 e), because of dominant polarization effects. The latter become less important than charge transfer when the number of ligands increases. For a given size of aggregate, q_N becomes *less* negative with Yb^{3+} than with La^{3+}, following the charge transfer to the cation rather than polarization effects.

The geometry perturbations of MeCN molecules depend on the cation's size and coordination number (Tables 2 and 3). They are largest in the smallest aggregates and increase with the cation hardness (from La^{3+} to Yb^{3+}). We notice (Table 2) that C≡N and C−Me distances in $Eu(MeCN)_5^{3+}$ are approximately the same as in the free ligand. In smaller aggregates (n < 5), C≡N is longer, whereas in higher aggregates (n > 5), C≡N is shorter, in full agreement with spectroscopic observations where MeCN coordination to M^{3+} cations leads to a shift to higher frequencies in solution.[42] Thus, shifts of vibrational frequencies in the condensed phase, where the first coordination shell is saturated, do not follow those of unsaturated complexes, where polarization effects are magnified.

The optimized $La(MeCN)_9^{3+}$ and $Yb(MeCN)_8^{3+}$ complexes (Figure 9 and Table 3) can be compared with the corresponding X-ray structures (Table S3).[25] In both complexes, the calculated $MeCN\cdots M^{3+}$ distances are about 0.08 Å longer than in the crystal. About 0.05 Å of this difference may be ascribed to environment effects in the condensed phase, as suggested by calculations on lanthanide[43] and actinide[44] complexes "in solution" (mimicked by a reaction field correction). Without imposing any symmetry, the structures converged to symmetrical forms (D_{3h} and D_{4d}, respectively). We notice that in all three $M(MeCN)_9^{3+}$ complexes the three equatorial distances are somewhat longer than the six apical ones, following the same trend as in the solid-state structures.

The $Yb(MeCN)_9^{3+}$ complex, optimized starting from the optimized $Eu(MeCN)_9^{3+}$ one, retained a D_{3h} symmetry (Table 2). Because the coordination number of nine for Yb^{3+} is larger than the value observed in the crystal, we decided also to optimize a $Yb(MeCN)_{8+1}^{3+}$ complex. The latter was built from $Yb(MeCN)_8^{3+}$ of D_{4d} symmetry to which a ninth ligand was added in the second shell along a C'_2 symmetry axis. After minimization at the HF level, the coordination remained of 8+1 type (Figure 9 and Table 3), leading to a species more stable than $Yb(MeCN)_9^{3+}$ D_{3h} (ΔE = 4.0 kcal/mol). Repeating the geometry optimization of the 9 and 8+1 coordinated species at the DFT level yields a smaller ΔE (1.7 kcal/mol) and structures somewhat more compact (Yb...N distances are about 0.03 Å

TABLE 2: $Eu(MeCN)_n^{3+}$ Aggregates Optimized by QM and MD Calculations (Distances and Atomic (Mulliken) Charges)

	MeCN	$Eu(MeCN)_n^{3+}$								
n	1	1	2	3	4	5	6	8	9	15
		QM calculations: Optimized distances (Å) and mulliken charges								
symmetry	$C_{\infty v}$	$C_{\infty v}$	$D_{\infty h}$	C_{3v}[a]	T_d	D_{3h}	O_h	D_{4d}	D_{3h}	
d Eu···N	−	2.192	2.320	2.334	2.376	2.417/2.449[b]	2.475	2.560	2.639/2.592[c]	−
d C≡N	1.152	1.173	1.163	1.158	1.155	1.152/1.151[b]	1.149	1.147	1.146/1.146[c]	−
d C−C	1.468	1.456	1.463	1.466	1.467	1.468/1.468[b]	1.469	1.470	1.470/1.470[c]	−
q_N	−0.100	−0.645	−0.497	−0.494	−0.431	−0.322/−0.282[b]	−0.233	−0.147	−0.100/−0.094[c]	−
q_C	−0.020	+0.445	+0.298	+0.303	+0.249	+0.154/+0.128[b]	+0.090	+0.047	+0.034/+0.015[c]	−
q_{Me}	+0.120	+0.429	+0.368	+0.334	+0.304	+0.279/+0.273[b]	+0.253	+0.214	+0.194/0.200[c]	−
q_{Eu}	−	+2.772	+2.662	+2.572	+2.509	+2.433	+2.345	+2.091	+1.895	−
		MD (AMBER) simulations: average distances (Å)								
d $Eu^{3+}\cdots N$[d]	−	2.475	2.478	2.487	2.491	2.506	2.513	2.581	2.627	2.660
d $Eu^{3+}\cdots N$[e]	−	2.320	2.329	2.352	2.366	2.387	2.408	2.495	2.560	2.543

[a] The optimization started with a D_{3h} complex and converged to a C_{3v} symmetry. [b] Equatorial/axial MeCN. [c] Equatorial/apical MeCN. [d] With *set2*. [e] With *set2*+*pol*.

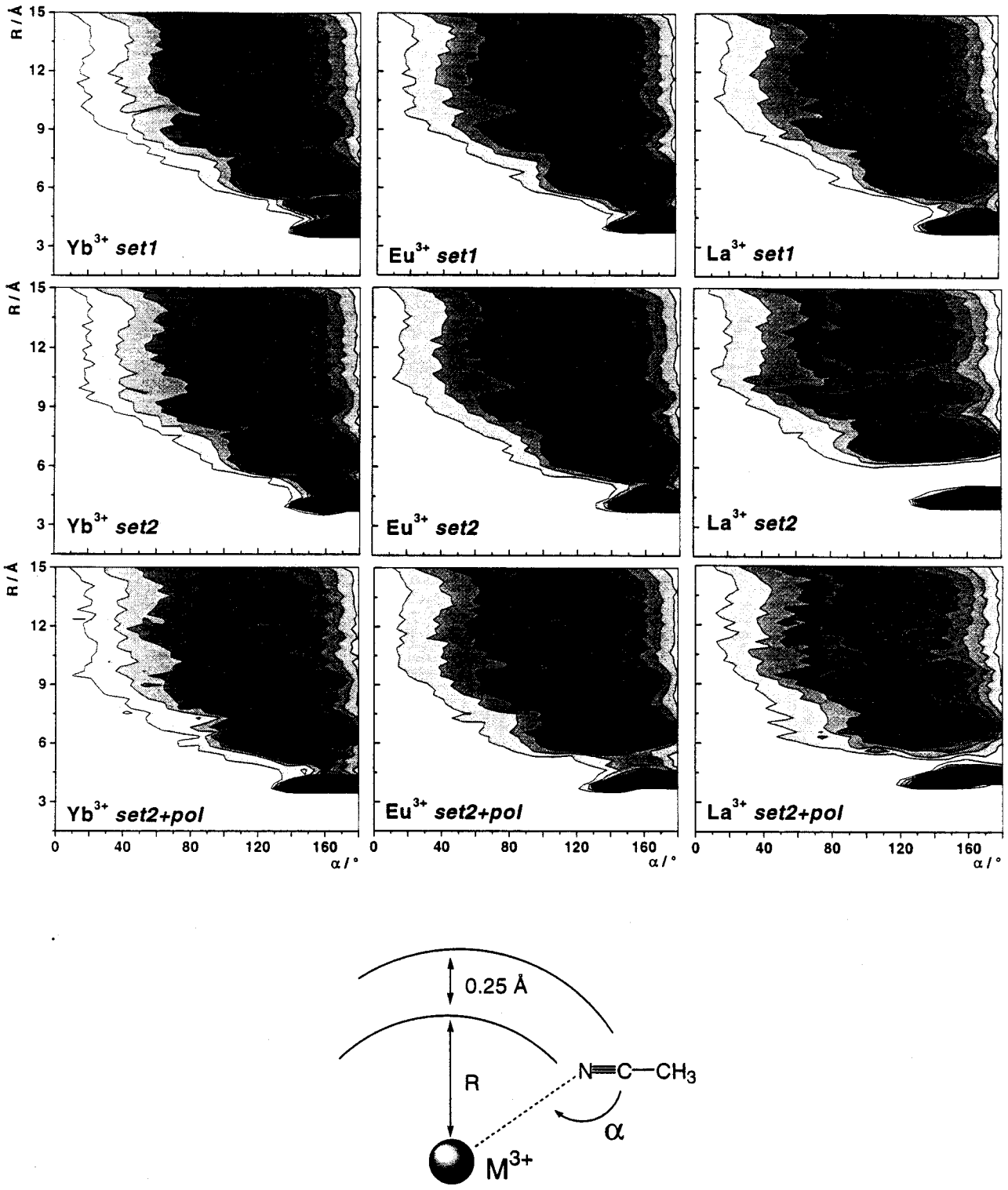

Figure 8. Orientation of MeCN solvent molecules around M^{3+} cations in acetonitrile (no counterions): population of configurations for given (*R*, α) values (*R* distance, Å, in ordinate and α-angle, degrees, in abscissa). Simulations with *set1*, *set2*, and *set2+pol*. Normalized populations are coded from 0.000 (white) to 0.006 (black). A color version of this figure is given as Supporting Information (Figure S1).

shorter) than those optimized at the HF level. These QM calculations confirm that the preferred coordination number of Yb^{3+} is eight, and that $Yb(MeCN)_9^{3+}$ likely corresponds to a transition state for ligand exchange, energetically close to the "ground state".

Concerning the comparison of $Eu^{3+}\cdots N$ distances in the QM vs MD optimized $Eu(MeCN)_9^{3+}$ aggregate, there is good agreement with the *set2* parameters (differences are less than 0.03 Å). The agreement with X-ray extrapolated data is better than in pure liquid solution or in $Eu(MeCN)_{15}^{3+}$ (Figure 7), where the cation coordination numbers are higher. In smaller aggregates, QM distances are much smaller than MD ones because of the polarization effects described above, whereas in saturated aggregates, QM and MD converge to similar values. Thus, *force-field parameters to be used in condensed phases should not be fitted on unsaturated complexes*.

Some energy features of the $M(MeCN)_n^{3+}$ aggregates obtained from different methods are illustrated in Figure S3 as a

TABLE 3: $La(MeCN)_n^{3+}$ and $Yb(MeCN)_n^{3+}$ Aggregates (n = 1, 8, and 9) Optimized by HF QM Calculations[a]

	OPLS	QM calculations						
	MeCN	$La(MeCN)_n^{3+}$			$Yb(MeCN)_n^{3+}$			
n	1	1	8	9	1	8	9	8+1
symmetry	$C_{\infty v}$	$C_{\infty v}$	D_{4d}	D_{3h}	$C_{\infty v}$	D_{4d}	D_{3h}	C_1
d M···N	−	−	2.669	2.728/2.703[b]	2.097	2.468	2.583/2.495[b]	2.465/6.060[c]
d C≡N	1.157	1.152	1.148	1.147/1.147[b]	1.174	1.146	1.146/1.145[b]	1.146/1.155[c]
d C−C	1.458	1.468	1.470	1.470/1.470[b]	1.454	1.470	1.470/1.470[b]	1.469/1.472[c]
q_N	−0.43	−0.100	−0.192	−0.144/−0.139[b]	−0.622	−0.111	−0.069/−0.068[b]	−0.110/−0.226[c]
q_C	+0.28	−0.020	+0.041	+0.030/+0.010[b]	+0.457	+0.055	+0.028/+0.024[b]	+0.059/+0.050[c]
q_{Me}	+0.15	+0.120	+0.218	+0.201/+0.205[b]	+0.441	+0.207	+0.187/+0.193[b]	+0.200/+0.194[c]
q_M	−	−	+2.457	+2.288	+2.724	+1.793	+1.664	+1.789

[a] Data for the uncomplexed MeCN molecule (OPLS model and QM optimized) is given for comparison. Distances and atomic (Mulliken) charges. [b] Equatorial/apical MeCN. [c] First shell/second shell MeCN molecules.

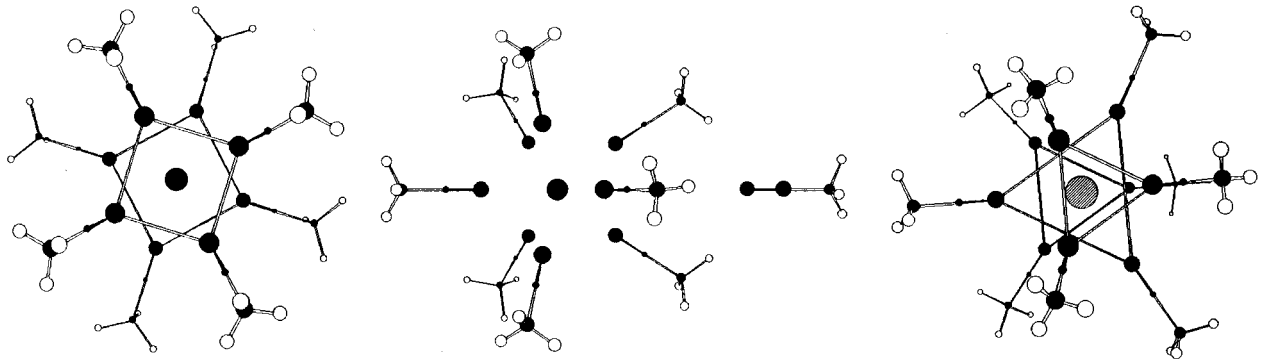

Figure 9. Optimized structures of $Yb(MeCN)_9^{3+}$ (D_{4d} symmetry), $Yb(MeCN)_{8+1}^{3+}$ (no symmetry), and $La(MeCN)_9^{3+}$ (D_{3h} symmetry).

function of n for the *set2* and *set2+pol* MD results (n = 1−15) and for the QM results (n = 1−6, 8, and 9). All methods show qualitatively that addition of one MeCN molecule to a $M(MeCN)_{n-1}^{3+}$ aggregate is energetically favorable, although starting to reach a plateau at n = 10. Compared with QM stabilization energies ΔE, MD values are underestimated for the smallest n, but become similar at n = 6, because of a compensation of the increasing cation/ligand(s) attractions and ligand−ligand repulsions. Among the MD results, ΔE is larger with the *set2+pol* than with the *set2* parameters before saturation of the first coordination shell, but becomes comparable after saturation.

2. MX_3 Salts in Acetonitrile: Ion Pairing and Cation Solvation. Where Are the Anions? From Dissociated to Intimate Ion Pairs. In acetonitrile solution, many anions interact with lanthanide cations. According to Bünzli et al.,[42,45] the apparent stability constants ($\mathrm{Log}K_1$) for the formation of monoperchlorato species in 0.05 M anhydrous acetonitrile solutions of $M(ClO_4)_3$ are in the order of 2.0, and increase by about 0.5 unit from Tb^{3+} to Yb^{3+}. For tris-triflate species formed in solutions of $M(F_3CSO_3)_3$ salts, $\mathrm{Log}K_3$ is in the order of 2.5 and the number of uncoordinated anions is greater than two.[45] Conductometric measurements show $M(ClO_4)_3$ (M = Nd, Eu, Er) to be 2:1 electrolytes in anhydrous acetonitrile,[46] whereas $Yb(F_3CSO_3)_3$ is a 1:1 electrolyte.[3] In anhydrous acetonitrile, only the heavier lanthanide complexes are soluble, and according to IR spectroscopy studies of $M(ClO_4)_3$ salts, the number of coordinated perchlorate anions ranges from 1.6 (for La^{3+}) to 0.9 (for Yb^{3+}).[3,47−49] We therefore decided to simulate some of these salts, to gain insights into the question of ion pairing, focusing mainly on the extreme cases, that is, Yb^{3+}(*set1*) and La^{3+}(*set2*).

TABLE 4: $M(ClO_4)_3$ and $M(F_3CSO_3)_3$ Salts Simulated in Acetonitrile[a]

salt	binding mode[b]	N_O	N_{MeCN}	CN_{total}
$Yb(ClO_4)_3$ *set1*	*m*	3.0	5.0 + 1.0	9.0
$La(ClO_4)_2^+$ *set2*	*m*	2.0	10.0	12.0
$La(ClO_4)_3$ *set2*	*m*	3.0	9.0	12.0
$Yb(F_3CSO_3)_3$ *set1*	*b*	6.0	2.0	8.0
$La(F_3CSO_3)_3$ *set2*	*t, (b)*	8.5	3.3	11.8

[a] Number N_O of coordinated O atoms of the anion, and number N_{MeCN} of coordinated MeCN molecules. The total coordination number is $CN_{total} = N_O + N_{MeCN}$. [b] The *m* stands for monodentate, *b* for bidentate, and *t* for tridentate binding mode of the anions.

We first conducted several MD simulations, ranging from 0.2 to 1.6 ns, which started with intimate 1:3 ion pairs, to test whether they spontaneously dissociate to complexes of lower stoichiometries. In contrast to what was simulated in water,[50,51] all salts remained fully associated, as previously found for the $Eu(NO_3)_3$ or Eu(Picrate)$_3$ salts in acetonitrile.[50] It is unclear whether such association results from a thermodynamic equilibrium, or from a metastable state trapped by a dissociation energy barrier too high to be overcome at 300 K.

We therefore proceeded to other tests, starting with fully dissociated M^{3+}/X^- ion pairs, to investigate whether these ions would spontaneously pair in acetonitrile. Two typical examples are given in Figure 10, for the smallest Yb^{3+}(*set1*) and largest La^{3+}(*set2*) ions, respectively. These simulations started with ClO_4^- or $F_3CSO_3^-$ anions at about 12 Å from the cations (i.e., at 3 Å less than the cutoff distance), forming X−M−X angles of about 120°. Although the Coulombic interactions were similar in all starting systems, the systems evolved somewhat differently. The Yb^{3+} perchlorate or triflate salts and the La^{3+} triflate

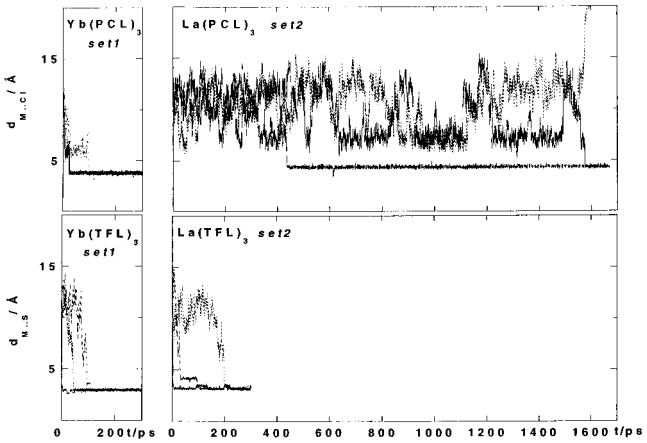

Figure 10. Perchlorate (PCL) and triflate (TFL) salts of Yb^{3+}(*set1*) and La^{3+}(*set2*) cations in acetonitrile: M^{3+}···anion distances (Å) as a function of time (ps). The MD simulations start with fully dissociated ion pairs. A color version of this figure is given as Supporting Information (Figure S2).

salt rapidly formed intimate ion pairs (in less than 200 ps), leading to $M(ClO_4)_3$ and $M(F_3CSO_3)_3$ species, respectively. In La^{3+} perchlorate, ion pairing was slower and partial only. A first ClO_4^- anion coordinated to La^{3+} at about 450 ps, a second one at 1.6 ns, whereas the third one dissociated beyond the cutoff distance to the bulk. These simulations are not sufficient to conclude on the stability of ion pairs either, because the trajectories are driven by the potential energy, as well as by the velocities of ions and molecules. We performed other simulations, starting at lower M^{3+}···X^- distances (about 7 Å), or resetting the velocities to random values along the dynamics, or starting with partially formed pairs (e.g., MX_2^+). Other tests used the PME Ewald method to take into account the long-range electrostatic interactions. No firm conclusion could be obtained, because most of them converged to different types of ion pairs, where the anions were partially bound. The "reality" is likely an equilibrium between the different states, which remains a challenge for future computational approaches.

Solvation and Structure of $M(ClO_4)_3$ and $M(F_3CSO_3)_3$ Salts Forming Intimate Ion Pairs. In all cases, the cation of the associated 1:3 salts is solvated by additional MeCN molecules, leading to somewhat different binding and solvation patterns depending on the anion type, cation size, and model. Typical structures of the Eu^{3+} salts are shown in Figure 11 and typical cation coordination numbers (N_O of anionic oxygen atoms and N_{MeCN} of acetonitrile molecules) are summarized in Table 4. With the *set1* and *set2* calculations, the three perchlorate anions are mostly monodentate, allowing for coordination of six (Yb^{3+},*set1*) to nine (La^{3+},*set2*) MeCN molecules. This binding mode somewhat differs from the one inferred from IR spectroscopic studies, according to which ClO_4^- anions coordinate mono- and bidentately.[3] Such discrepancy has already been noticed with NO_3^- counterions.[51,52] The latter are generally considered to be bidentate, whereas according to the MD simulations in aqueous solution, they are monodentate.[51]

The simulated triflate anions display mono-, bi-, and tridentate binding to Eu^{3+} (Figure 11), whereas the number of coordinated MeCN molecules is generally lower than with ClO_4^-: from 2 with Yb^{3+}(*set1*) to 3 with La^{3+}(*set2*). To our knowledge, the corresponding binding patterns have not been investigated experimentally.

Taking into account polarization (*set2*+*pol*) favors bis- and even tridentate coordination modes of both ClO_4^- and $F_3CSO_3^-$ anions. As a result, the number of coordinated MeCN molecules drops by one to two units, relative to the *set2* results.

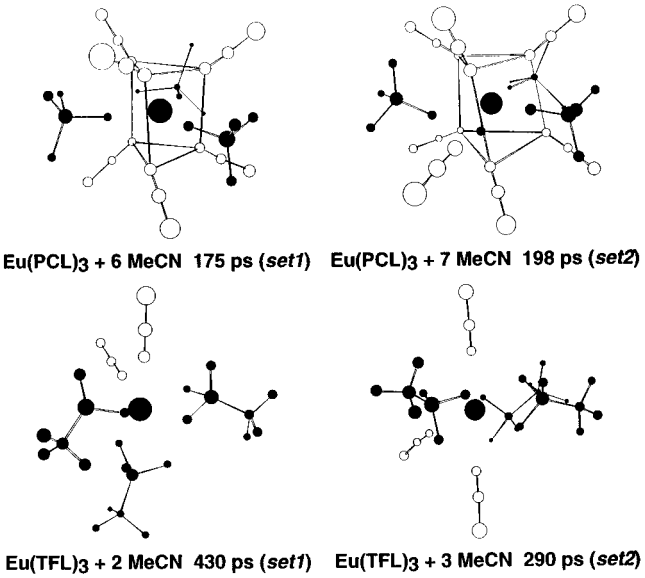

Figure 11. First coordination shell of Eu^{3+} in the perchlorate (PCL) and triflate (TFL) salts simulated in solution with the *set1* and *set2* models.

3. Relative Free Energies of Solvation of M^{3+} Cations in Acetonitrile. The Role of the Model and of X^- Counterions. In this section, based on FEP calculations, we investigate the role of cation model (*set1* vs *set2*) and solvent model (*set2* vs *set2*+*pol*) on the changes in solvation free energies ΔG_3 from one cation to the other (La^{3+} vs Eu^{3+} and Eu^{3+} vs Yb^{3+}) in dry acetonitrile solution. First, the cations are modeled without counterions and the changes in free energies are compared with those obtained in $M(MeCN)_{15}^{3+}$ aggregates. Then the role of counterions is investigated in solutions of MX_3 and MX_1^{2+} salts forming intimate ion pairs. Results are reported in Table 5. In all cases, ΔG_3 becomes more positive when the size of the cation increases (Yb^{3+} < Eu^{3+} < La^{3+}), following trends of the lanthanide, alkaline-earth, and alkali cation hydration energies.[53]

Changes in Free Energies of Solvation of M^{3+} Cations (No Counterions). The difference ΔG_3 between two consecutive cations amounts to about 30 kcal/mol with both *set1* and *set2* models, and to about 50 kcal/mol with the *set2*+*pol* model. These numbers are lower than, or comparable to the differences in the corresponding hydration energies.[53] The differences between *set1* and *set2* results are small. For instance, for the $Eu^{3+} \rightarrow La^{3+}$ mutation, ΔG_3 is 33.2 and 34.1 kcal/mol, respectively. Adding polarization on MeCN (*set2*+*pol*) leads to a spectacular increase of ΔG_3 (by about 24 kcal/mol for the $Eu^{3+} \rightarrow La^{3+}$ mutation and 21 kcal/mol for the $Yb^{3+} \rightarrow Eu^{3+}$ mutation). Another interesting observation is the similarity of the ΔG_3 energies in the pure liquid and in the $M(MeCN)_{15}^{3+}$ aggregates (Table 5) with all three models. The ΔG_3 values are only 0.4 to 3.0 kcal/mol larger in the liquid than in the aggregate, likely due to the contribution of MeCN molecules of the second or intermediate shells. The changes in cation coordination numbers are also very similar in the two systems.

Changes in Free Energies of Solvation of MX_3 and MX^{2+} Salts. The role of neutralizing counterions on the relative free energies of lanthanide cation solvation ΔG_3 has been examined with the three models, for MX_3 and MX^{2+} salts.

We first discuss the neutral MX_3 salts (Table 5). Adding three counterions to the naked M^{3+} cation leads to an increase of the ΔG_3 energies, the largest effects being observed with triflate

TABLE 5: Differences in Free Energies (kcal/mol) from FEP Calculations on M^{3+} Cations, MX_n^{3-n} salts, ML_3^{3+} and ML_3X_3 Complexes

	ΔG_3 (uncomplexed cation)		$\Delta\Delta G_{ass}$[b]		ΔG_4 (complexed cation)		$\Delta\Delta G_c$	
	Yb→Eu	Eu→La	Eu	Yb	Yb→Eu	Eu→La	Eu	Yb
experiment							−1.8	−2.5
	M^{3+}				ML_3^{3+}		ML_3^{3+}	
set1	25.7	33.2			33.3	49.7	−16.5	−24.1
					(33.0)[d]	(50.7)[d]		
set2	30.4	34.1			44.3	48.2	−14.1	−28.0
	(29.8)[c]	(31.1)[c]			(44.4)[d]	(59.0)[d]		
set2+pol	51.2	58.3					−16.1	−20.7
	(50.3) [c]	(56.7) [c]			(55.8) [d]	(74.4) [d]		
	$M(ClO_4)_1^{2+}$		$M(ClO_4)_1^{2+}$				$ML_3\,(ClO_4)_1^{2+}$	
set1	27.8	35.5	−2.3	−4.4			−14.2[e]	−19.7[e]
set2	31.9	36.3	−2.2	−3.7			−11.9[e]	−24.3[e]
set2+pol	66.9	70.2	−11.9	−27.6			−4.2[f]	+6.9[f]
	$M(ClO_4)_3$		$M(ClO_4)_3$		$ML_3\,(ClO_4)_3$		$ML_3\,(ClO_4)_3$	
set1	31.5	39.4	−6.2	−12.0	32.6	44.3	−4.9	−6.0
set2	35.3	40.2	−6.1	−11.0	42.3	48.0	−7.8	−14.8
set2+pol	78.4	80.3	−22.0	−49.2			+5.9	+28.5
	$M(F_3CSO_3)_1^{2+}$		$M(F_3CSO_3)_1^{2+}$				$ML_3\,(F_3CSO_3)_1^{2+}$	
set1	33.3	41.1	−7.9	−15.5			−8.6[e]	−8.6[e]
set2	36.8	40.4	−6.3	−12.7			−7.8[e]	−15.3[e]
set2+pol	73.8	77.9	−19.6	−42.2			+3.5[f]	+21.5[f]
	$M(F_3CSO_3)_3$		$M(F_3CSO_3)_3$		$ML_3\,(F_3CSO_3)_3$		$ML_3\,(F_3CSO_3)_3$	
set1	46.8	51.7	−18.5	−39.6	34.8[g]	45.2[g]	+6.5	+18.5
					41.1[h]	51.3[h]	+0.4	+6.1
set2	47.8	52.7	−18.6	−36.0	42.1	50.8	+1.9	+7.6
set2+pol	88.6	89.7	−31.4	−68.8			+15.3	+48.1

[a] Unless otherwise specified, the simulations are performed in acetonitrile solution. The $\Delta\Delta G_{ass}$ and $\Delta\Delta G_c$ energies are relative to La^{3+}. These energy differences, ΔG_3 and ΔG_4, are defined in the text, based on Schemes 1 and 2. All values in kcal·mol^{-1}, errors estimated between forward and backward calculations are 0.4 kcal·mol^{-1}. [b] Difference in free energy due to the addition of counterions, relative to La^{3+}. See Scheme 1 for definition. [c] Values in parentheses are calculated for $M(MeCN)_{15}^{3+}$ clusters. [d] Values in parentheses are calculated in vacuo. [e] ML_3^{3+} complex without counterions vs $M(X)_1^{2+}$ salt. [f] ML_3^{3+} complex without counterions (in vacuo) vs $M(X)_1^{2+}$ salt. [g,h] Two starting situations have been investigated for the complexes of the triflate salt: one with all 3 anions within the cutoff distance ([g]), and another one with only two triflates within the cutoff of M^{3+} ([h]).

anions, which display larger interactions than the perchlorate anions with the coordinated cations. For instance, with the *set1* parameters, the ΔG_3 difference between Yb^{3+} and La^{3+} increases from 59 kcal/mol (no counterions) to 71 kcal/mol (with ClO_4^- anions) and 98 kcal/mol (with $F_3CSO_3^-$ anions). With the *set2* parameters, the corresponding energy changes are similar (about 64, 75, and 99 kcal/mol, respectively). Thus *changes $\Delta\Delta G_3$ induced by the anion coordination to the cation are much larger than those observed from one cation model to the other.*[54]

Taking into account polarization of the solvent and of the coordinated anions (*set2+pol* parameters) leads to spectacular increase of ΔG_3 energies, the effect being again larger with $F_3CSO_3^-$ than with ClO_4^- anions. The ΔG_3 energy difference between Yb^{3+} and La^{3+} increases from 109 kcal/mol (no counterions) to 159 kcal/mol (with ClO_4^- anions) and 178 kcal/mol (with $F_3CSO_3^-$ anions). These energies are nearly twice as large as those obtained without polarization (*set2*). This stems from the fact that the anions are more tightly bound with the *set2+pol* than with the *set2* model and that they have higher atomic polarizabilities than the solvent molecules. If one refers to the anion coordination inferred from spectroscopic studies,[3] it appears that the calculations overestimate the extent of anion binding to M^{3+}, and that this artifact increases when polarizabilities of the solvent and anions are added to the force field.

Because a 1:3 coordination is likely exaggerated, we decided to also simulate 1:1 complexes of $M(ClO_4)_1^{2+}$ and $M(F_3CSO_3)_1^{2+}$ type, and to calculate the change in free energies from one cation to the other. The results (Table 5) follow the same trends as for the 1:3 salts. There is little difference between the *set1* and *set2* energies, whereas the *set2+pol* values are again about twice as high. For a pair of cations, the ΔG_3 energies increase upon addition of counterions: "naked cation" < $M(X)_1^{2+}$ < $M(X)_3$.

SCHEME 1

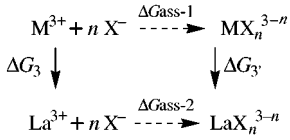

Insights into differences in ion pairing may be obtained from differences in association energies $\Delta\Delta G_{ass}$ for M^{3+} vs La^{3+} cations to a same anion X^-. According to the above cycle (Scheme 1), $\Delta\Delta G_{ass} = \Delta G_{ass-1} - \Delta G_{ass-2} = \Delta G_3 - \Delta G_3'$, where ΔG_3 and $\Delta G_3'$ are the differences in solvation energies between the two "naked" cations and the anion−cation pairs, respectively.

The energies reported in Table 5 confirm the conclusions above: with all sets of parameters, counterion effects on $\Delta\Delta G_{ass}$ energies are larger for $F_3CSO_3^-$ than for ClO_4^- anions. They are roughly proportional to the number of coordinated anions X^- and similar with *set1* and *set2* parameters. Adding polarization (*set2+pol*) markedly enhances the energy differences (by a factor of about 4 with ClO_4^-, and 2 with $F_3CSO_3^-$)[55].

4. Cation Complexation in Acetonitrile: Comparison of Simulated vs Experimental Structures and Binding Selectivities of ML_3^{3+} Complexes (L = Pyridine−dicarboxamide). The effect of cation representation was investigated in a ML_3^{3+} complex where **L** is a pyridine−dicarboxamide ligand (Figure

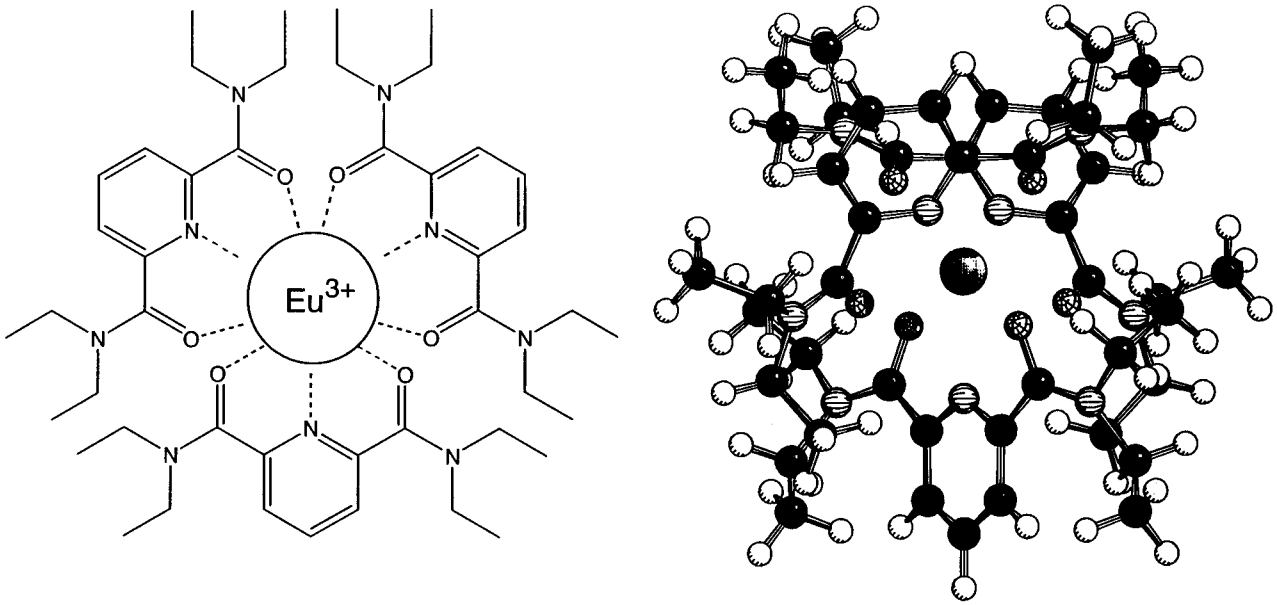

Figure 12. The Eu$\mathbf{L}_3^{3+}$ complex of the pyridine−dicarboxamide ligand **L**: schematic view (left) and X-ray structure (right).

SCHEME 2

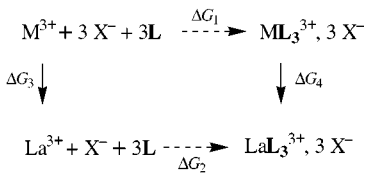

12) whose structure and cation binding selectivity have been characterized experimentally.[56]

Structural Data. According to X-ray data (Table S4), average $M-O_L$ distances are somewhat shorter than the M−N distances (by about 0.15 Å in the La^{3+} complex, and 0.10 Å in the Eu^{3+} complex). They are also about 0.10−0.14 Å shorter with Eu^{3+} than with La^{3+}. In a given complex, M−O and M−N distances display variations of up to 0.06 Å. These trends are reproduced by all calculations (Table S4) and, as expected, all distances are somewhat larger with *set2* than with *set1*. The comparison of in vacuo vs acetonitrile solution simulations performed with *set1* shows that the simulation phase has little influence on the cation−ligand distances; they deviate by 0.01 Å in the Eu^{3+} complex and by about 0.03 Å in the La^{3+} complex, because of the transient coordination of one solvent molecule to La^{3+} in solution. Both sets or cation parameters yield reasonable agreement with experimental structures, but average M−O and M−N distances are somewhat too long with *set2* (by about 0.20 Å in the La^{3+} complex and 0.05 Å in the Eu^{3+} complex). Taking into account the polarization (*set2*+*pol*) in gas-phase simulations improves the agreement with experiment, excepted for the La−O distances which remain too long by about 0.08 Å.

Binding Selectivities. We now consider the question of ion binding selectivity $\Delta\Delta G_c$ between M_1^{3+} and M_2^{3+} cations, defined experimentally by $\Delta G_1 - \Delta G_2$. According to ref 56, the ligand **L** forms strong complexes with lanthanide cations in acetonitrile, whose stability slightly increases with the atomic number ($\log\beta_3$ is 21.0 for La^{3+}, 22.3 for Eu^{3+}, and 22.8 for Yb^{3+}). It is thus challenging to reproduce this trend. The computer simulations use the "alchemical route" and calculate $\Delta\Delta G_c$ as $\Delta G_3 - \Delta G_4$ (Scheme 2), where ΔG_3 is the difference in the free energies of solvation of the uncomplexed cations and ΔG_4 corresponds to the difference in free energies of the complexes.

For the uncomplexed state, we used the ΔG_3 values reported above, considering different states for the counterions. The *set1* and *set2* calculations of ΔG_4 were performed in solution with explicit counterions, whereas for the *set2*+*pol* calculations we calculated ΔG_4 in the gas phase without counterions, for computer time-saving purposes.[56,57] The results are reported in Table 5.

When the uncomplexed cation is considered without counterions, combination of ΔG_3 and ΔG_4 energies yields the correct order of binding selectivities ($La^{3+} < Eu^{3+} < Yb^{3+}$) with the three models. The $\Delta\Delta G_c$ energies are comparable with *set1*, *set2*, and *set2*+*pol* (21−28 kcal/mol for $La^{3+} \rightarrow Yb^{3+}$) and markedly exaggerated, compared with the experimental value of 2.5 kcal/mol.[56]

When X^- counterions are taken into account for the uncomplexed states (MX_3 associated salt), the situation is more complicated. With $F_3CSO_3^-$, all three models yield the same order, which is incorrect and opposite to the experimental one, the worse results being obtained with the *set2*+*pol* model ($\Delta\Delta G_c$ = +48.1 kcal/mol for $La^{3+} \rightarrow Yb^{3+}$). The changes from *set1* to *set2* are much smaller than those from *set2* to *set2*+*pol*. With ClO_4^- as counterions the trend in $\Delta\Delta G_c$ values is correct (but exaggerated) with *set1* and *set2*, but incorrect with the *set2*+*pol* model. Thus, addition of polarization energies leads to erroneous predictions of binding selectivities. On the other hand, for a given system, both *set1* and *set2* yield similar qualitative conclusions, indicating that the latter are not critically determined by small changes in the size of M^{3+}. It appears from Table 5 that erroneous predictions of the selectivities stems from the exaggeration of ΔG_3 energies of the uncomplexed cations, rather than from the ΔG_4 energies of the $M\mathbf{L}_3^{3+}$ complexes. Whether this is caused by the particular choice of atomic polarizabilities,[58] by inconsistencies between atomic charges and polarizabilities, or by the neglect of charge-transfer and many-body interactions remains to be investigated.

Given the overestimation of cation−anion association in acetonitrile with all models, we decided to also consider the 1:1 MX^{2+} salts as reference state to estimate ΔG_3 (see Table 5). The predicted order of binding selectivities is the experimental one with *set 1* and *set2*, for both types of counterions, and the numbers, still exaggerated, are closer to the experimental ones. Again, with the *set2*+*pol* model, the trend is inverted,

because of the overestimation of the ΔG values of the uncomplexed state compared with the complexed one.

IV. Discussion and Conclusion

We report theoretical MD and QM investigations on the solvation and complexation properties of La^{3+}, Eu^{3+}, and Yb^{3+} cations in acetonitrile solution and in $M(MeCN)_n^{3+}$ aggregates, mainly to test to what extent cation parameters (*set2*) developed from their hydration properties also properly describe these cations in another solvent, using simple pairwise additive 1−6−12 potentials. The *set2* is compared with *set1* cation parameters, obtained by scaling down the van der Waals cation radius R^* by $2^{1/6}$. The role of solvent and anion polarization effects is investigated with the *set2*+*pol* model.

For the uncomplexed cations, in the absence of counterions, *set2* overestimates the cation coordination numbers, whereas *set1* leads to closer agreement with available experimental data, both in terms of coordination numbers and distances. Quantum mechanical optimizations of the $M(MeCN)_n^{3+}$ aggregates demonstrate the importance of charge-transfer and polarization effects. Adding a polarization energy term (*set2*+*pol* parameters) improves the MD results and yields reasonable coordination numbers of M^{3+} in the absence of accompanying anions. With all three models, the rate of solvent exchange in the first coordination shell *increases* from La^{3+} to Yb^{3+}, following a trend opposite to the ion−solvent interaction energies, and opposite to aqueous solution. This feature, similar to the one observed with dimethylformamide (DMF) solutions of lanthanide cations,[59] would be worth investigating experimentally in acetonitrile. Concerning the smallest simulated cation (Yb^{3+}), our QM results confirm that in the gas phase the coordination number of eight is energetically preferred, compared with a coordination number of nine, but the difference is quite small (4.0 kcal/mol at the HF level and 1.7 kcal/mol at the DFT level).

Another series of simulations deals with the MX_3 salts in acetonitrile, where $X^- = ClO_4^-$ vs $F_3CSO_3^-$ anions are compared. All three models seem to overestimate the cation−anion interactions, with respect to the cation−solvent attractions, and the differences between the *set1* and *set2* results are small, compared with differences between *set2* and *set2*+*pol* results. The latter lead to worse agreement between calculated and experimental anion-binding modes, indicating that polarization exaggerates cation−anion interactions compared with cation−solvent ones. Taken together, all simulations point to the *role of counterions on the free energies of complexation* by a ligand.

A recent paper on the solvation of Rb^+ and Sr^{2+} ions in acetonitrile using 1−6−12 parameters fitted on hydration free energies (no polarization and no counterions) reports a satisfactory agreement between calculated coordination numbers, compared with the values determined by X-ray absorption spectroscopy.[60] With the trivalent cations, polarization effects are too large to be neglected, and cation parameters fitted from hydration properties poorly describe the cation solvation in acetonitrile. The role of counterions has also to be taken into account.

The importance of counterions is supported further by FEP simulations on $M\mathbf{L}_3^{3+}$ complexes of a pyridine−dicarboxamide ligand **L**, where qualitative trends in cation-binding selectivities are reproduced by the *set1*, *set2*, and *set2*+*pol* models without counterions. When counterions are considered in the uncomplexed state of M^{3+}, the results are more versatile. In particular, inclusion of polarization (*set2*+*pol)* leads to an erroneous order of binding selectivities, because of the exaggeration of relative solvation energies on the uncomplexed cations.

These results are important for complexation studies in nonaqueous solvents,[42] as well as for complexation by nitrogen-containing ligands, such as pyridine derivatives.

Taken together, these studies indicate that when using simple pairwise additive 1−6−12 potentials together with Lorentz−Berthelot mixing rules, the precise size of the cation is not crucial, and that using cation radii smaller than those derived from hydration properties yields better results in acetonitrile. Fixed charge models neglect electronic reorganization upon cation binding, including charge-transfer and polarization contributions. Because of computer time limitations, we limited the investigations to two-body interactions, adding a polarization term to the potential energy. This improves the description of the uncomplexed cations (no counterions), but leads to improper balance of solvent vs anion interactions with the cation, and to exaggerated binding of counterions, compared to the solvent molecules. Whether this results from inadequate choice of charges and representation of the polarizabilities remains to be investigated, including comparisons of united vs all atom models of the solvent and tests on more simple gas-phase systems.[61]

Acknowledgment. G.W., F.B., and M.B. are grateful to Université Louis Pasteur for computational resources and to CEA/DCC for support.

Supporting Information Available: Tables S1−S4 and Figures S1−S3 are provided as supplementary material. This material is available free of charge via the Internet at http://pubs.acs.org.

References and Notes

(1) Lehn, J. M. *Struct. Bonding* **1973**, *161*, 1−69.
(2) Rizkalla, E. N.; Choppin, G. R. In *Handbook on the Physics and Chemistry of Rare Earths. Lanthanides/Actinides: Chemistry*; Gschneider, K. A., Eyring, L., Choppin, G. R., Lander, G. H., Eds.; Elsevier Science: New York, 1994; pp 529−558.
(3) Bünzli, J.-C.; Milicic-Tang, A. In *Handbook on the Physics and Chemistry of Rare Earths*; Gschneider, Jr., K. A., Eyring, L., Eds.; Elsevier Science B. V.: New York, 1994; pp 306−359 and references therein.
(4) Lincoln, S. F. *Adv. Inorg. Bioinorg. Mech.* **1986**, *4*, 217−287.
(5) Impey, R. W.; Madden, P. A.; McDonald, I. R. *J. Phys. Chem.* **1983**, *87*, 5071−5083.
(6) Clementi, E. *Determination of Liquid Water Structure, Coordination Numbers for Ions and Solvation for Biological Molecules*; Springer-Verlag, Berlin, 1976.
(7) Heinzinger, K. *Pure Appl. Chem.* **1985**, *57*, 1031−1042.
(8) Galera, S.; Lluch, J. M.; Oliva, A.; Bertran, J.; Foglia, F.; Helm, L.; Merbach, A. E. *New J. Chem.* **1994**, *17*, 773−779.
(9) van Veggel, F. C. J. M.; Reinhoudt, D. *Chem. Eur. J.* **1999**, *5*, 90−95.
(10) Meier, W.; Bopp, P.; Probst, M. M.; Spohr, E.; Lin, J. I. *J. Phys. Chem.* **1990**, *94*, 4672−4682.
(11) Auffinger, P.; Wipff, G. *J. Am. Chem. Soc.* **1991**, *113*, 5976−5988.
(12) Kowall, T.; Foglia, F.; Helm, L.; Merbach, A. E. *J. Am. Chem. Soc.* **1995**, *117*, 3790−3799.
(13) Åqvist, J. *J. Phys. Chem.* **1990**, *94*, 8021−8024.
(14) Jorgensen, W. L.; Briggs, J. M. *Mol. Phys.* **1988**, *63*, 547−558.
(15) Berny, F.; Muzet, N.; Troxler, L.; Dedieu, A.; Wipff, G. *Inorg. Chem.* **1999**, *38*, 1244−1252.
(16) Yamaguchi, T.; Nomura, M.; Wakita, H.; Ohtaki, H. *J. Chem. Phys.* **1988**, *89*, 5153−5159.
(17) Cossy, C.; Helm, L.; Powell, D. H.; Merbach, A. E. *New J. Chem.* **1995**, *19*, 27−35.
(18) Habenschuss, A.; Spedding, F. H. *J. Chem. Phys.* **1979**, *70*, 3758−3762.
(19) Habenschuss, A.; Spedding, F. H. *J. Chem. Phys.* **1979**, *70*, 2797−2806.
(20) Habenschuss, A.; Spedding, F. H. *J. Chem. Phys.* **1980**, *71*, 442−450.
(21) Rizkalla, E. N.; Choppin, G. R. In *Handbook on the Physics and Chemistry of Rare Earths*; Gschneidner, K. A., Eyring, L., Eds.; Elsevier Science: New York, 1991; pp 393−442.
(22) Hay, B. P. *Inorg. Chem.* **1991**, *30*, 2876−2884 and references therein.

(23) Shen, Q.; Hu, J.-Y.; Jin, Z.-S.; Sun, Y. *Zhongguo Xitu Xuebao (J. Chin. Rare Earth Soc.)* **1990**, *8*, 359.
(24) Hu, J.-Y.; Shen, Q.; Jin, Z.-S. *Chinese Sci. Bull.* **1990**, *35*, 1090−1092.
(25) Deacon, G. B.; Görtler, B.; Junk, P. C.; Lork, E.; Mews, R.; Petersen, J.; Zemva, B. *J. Chem. Soc., Dalton Trans.* **1998**, 3887−3891.
(26) Bünzli, J.-C.; Milicic-Tang, A. *Inorg. Chim. Acta* **1996**, *252*, 221−228.
(27) Pearlman, D. A.; Case, D. A.; Caldwell, J. C.; Seibel, G. L.; Singh, U. C.; Weiner, P.; Kollman, P. A. *AMBER4*; University of California: San Francisco, 1991.
(28) Cornell, W. D.; Cieplak, P.; Bayly, C. I.; Gould, I. R.; Merz, K. M.; Ferguson, D. M.; Spellmeyer, D. C.; Fox, T.; Caldwell, J. W.; Kollman, P. A. *J. Am. Chem. Soc.* **1995**, *117*, 5179−5197.
(29) Dang, L. X.; Rice, J. E.; Caldwell, J.; Kollman, P. A. *J. Am. Chem. Soc.* **1991**, *113*, 2481−2486.
(30) Applequist, J.; Carl, J. R.; Fung, K.-K. *J. Am. Chem. Soc.* **1972**, *94*, 4, 2952−2960.
(31) Engler, E.; Wipff, G. Unpublished work.
(32) Engler, E.; Wipff, G. In *Crystallography of Supramolecular Compounds*; Tsoucaris, G., Ed.; Kluwer: Dordrecht, 1996; pp 471−476.
(33) Frisch, M. J.; Trucks, G. W.; Schlegel, H. B.; Gill, P. M. W.; Johnson, B. G.; Robb, M. A.; Cheeseman, J. R.; Keith, T.; Petersson, G. A.; Montgomery, J. A.; Raghavachari, K.; Al-Laham, M. A.; Zakrzewski, V. G.; Ortiz, J. V.; Foresman, J. B.; Peng, C. Y.; Ayala, P. Y.; Chen, W.; Wong, M. W.; Andres, J. L.; Replogle, E. S.; Gomperts, R.; Martin, R. L.; Fox, D. J.; Binkley, J. S.; Defrees, D. J.; Baker, J.; Stewart, J. P.; Head-Gordon, M.; Gonzales, C.; Pople, J. A. *Gaussian 94, Revision B.2.*; Gaussian, Inc.: Pittsburgh, PA. 1995.
(34) Frisch, M. J.; Trucks, G. W.; Schlegel, H. B.; Scuseria, G. E.; Robb, M. A.; Cheeseman, J. R.; Zakrzewski, V. G.; Montgomery, J. A., Jr.; Stratmann, R. E.; Burant, J. C.; Dapprich, S.; Millam, J. M.; Daniels, A. D.; Kudin, K. N.; Strain, M. C.; Farkas, O.; Tomasi, J.; Barone, V.; Cossi, M.; Cammi, R.; Mennucci, B.; Pomelli, C.; Adamo, C.; Clifford, S.; Ochterski, J.; Petersson, G. A.; Ayala, P. Y.; Cui, Q.; Morokuma, K.; Malick, D. K.; Rabuck, A. D.; Raghavachari, K.; Foresman, J. B.; Cioslowski, J.; Ortiz, J. V.; Stefanov, B. B.; Liu, G.; Liashenko, A.; Piskorz, P.; Komaromi, I.; Gomperts, R.; Martin, R. L.; Fox, D. J.; Keith, T.; Al-Laham, M. A.; Peng, C. Y.; Nanayakkara, A.; Gonzalez, C.; Challacombe, M.; Gill, P. M. W.; Johnson, B.; Chen, W.; Wong, M. W.; Andres, J. L.; Gonzalez, C.; Head-Gordon, M.; Replogle, E. S.; Pople, J. A. *Gaussian 98; Revision A.5*; Gaussian, Inc.: Pittsburgh, PA, 1998.
(35) Dolg, M.; Stoll, H.; Savin, A.; Preuss, H. *Theor. Chim. Acta* **1993**, *85*, 441.
(36) Dolg, M.; Stoll, H.; Savin, A.; Preuss, H. *Theor. Chim. Acta* **1989**, *75*, 173.
(37) Ehlers, A. W.; Böhme, M.; Dapprich, S.; Gobbi, A.; Höllwarth, A.; Jonas, V.; Köhler, K. F.; Stegmann, R.; Veldkamp, A.; Frenking, G. *Chem. Phys. Lett.* **1993**, *208*, 111.
(38) Dunning, T. H.; Hay, P. J. In *Methods of Electronic Structure Theory. Modern Theoretical Chemistry 3*; Schaefer, III, H. F., Ed.; Plenum Press: New York, 1977; pp 1−28.
(39) Kaupp, M.; Schleyer, P. v. R. *J. Phys. Chem.* **1992**, *96*, 7316−7323.
(40) Cossy, C.; Merbach, A. E. *Pure Appl. Chem.* **1988**, *60*, 1785−1796.
(41) Allen, F. H.; Kennard, O. *Chem. Des. Autom. News* **1993**, *8*, 31−37.
(42) Bünzli, J.-C. G.; Milicic-Tang, A. *Inorg. Chim. Acta* **1982**, *252*, 221−228.
(43) Boehme, C.; Wipff, G. *Inorg. Chem.* **1999**, *38*, 5734−5741.
(44) Spencer, S.; Gagliardi, K.; Handy, N. C.; Ioannou, A. G.; Skylaris, C.-K.; Willetts, A.; Simper, A. M. *J. Phys. Chem. A* **1999**, *103*, 1831−1837.
(45) Bünzli, J.-C.; Milicic-Tang, A.; Mabillard, C. *Helv. Chim. Acta* **1993**, *76*, 1292−1305.
(46) Bünzli, J.-C. G.; Mabillard, C. *J. Less-Common Met.* **1986**, *126*, 379−388.
(47) DiBernardo, P.; Choppin, G. R.; Portanova, R.; Zanonato, P. *Inorg. Chim. Acta* **1993**, *12*, 85−91.
(48) Bünzli, J.-C. G.; Mabillard, C. *Inorg. Chem.* **1986**, *25*, 2750−2754.
(49) Bünzli, J.-C. G.; Kasparek, V. *Inorg. Chim. Acta* **1991**, *182*, 101−107.
(50) Wipff, G.; Troxler, L. In *Computational Approaches in Supramolecular Chemistry*; Wipff, G., Ed.; Kluwer: Dordrecht, 1994; pp 319−348.
(51) Beudaert, P.; Lamare, V.; Dozol, J.-F.; Troxler, L.; Wipff, G. *J. Chem. Soc., Perkin Trans.* **1999**, 2515−2524.
(52) Guilbaud, P.; Wipff, G., *J. Phys. Chem.* **1993**, *97*, 5685−5692.
(53) Marcus, Y. *Ion Solvation*; Wiley: Chichester, 1985.
(54) Of course, for a given cation, mutation of *set1* to *set2* parameters has a large effect on ΔG_3 (about 27 kcal/mol for Eu^{3+}), as expected from the scaled size of M^{3+}, but this question is less relevant than the comparison of two cations, which is much less model-dependent.
(55) The fact that these scaling factors strongly differ relates to structural effects: upon addition of polarization terms (from *set2* to *set2*+*pol*), the $F_3CSO_3^-$ anions remain mostly tridentate coordinated, whereas the ClO_4^- anions move from a monodentate to tridentate dominant binding modes.
(56) Renaud, F.; Piguet, C.; Bernardinelli, G.; Bünzli, J.-C. G.; Hopfgartner, G., *Chem. Eur. J.* **1997**, *3*, 1646−1659.
(57) The hypothesis according to which $\Delta G_{4(\text{solution})}$ and $\Delta G_{4(\text{gas})}$ energies are similar is reasonable, because the three **L** ligands wrap around the cation and shield it from the solvent and counterions, as supported by the X-ray structures of the La^{3+} and Eu^{3+} complexes,[56] by physical studies in acetonitrile,[56] and by comparative simulations.
(58) Ramnarayan, K.; Rao, B. G.; Singh, U. C. *J. Chem. Phys.* **1990**, *92*, 7057−7067.
(59) Pisaniello, D. L.; Helm, L.; Meier, P.; Merbach, A. E., *J. Am. Chem. Soc.* **1983**, *105*, 4528−4536.
(60) D'Angelo, P.; Pavel, N. V. *J. Chem. Phys.* **1999**, *111*, 5107−5115.
(61) Davidson, W. R.; Kebarle, P., *J. Am. Chem. Soc.* **1976**, *98* (8), 6125−6133.